ACS OMEGA

Open Access

This article is licensed under CC-BY-NC-ND 4.0

http://pubs.acs.org/journal/acsodf

Article

Cellulose Nanofibril Stabilized Pickering Emulsion Templated Aerogel with High Oil Absorption Capacity

Shuaib A. Mubarak, Yunsang Kim,* Islam Elsayed, and El Barbary Hassan

Cite This: *ACS Omega* 2023, 8, 36856−36867

Read Online

ACCESS | Metrics & More | Article Recommendations | Supporting Information

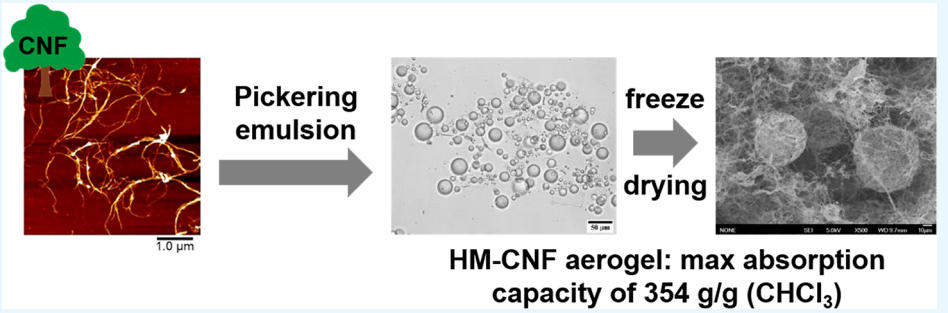

ABSTRACT: Nanocellulose-based aerogels, featuring a three-dimensional porous structure, are considered as a desirable green absorbent because of their exceptional absorption performance as well as the abundance and renewability of the raw material. However, these aerogels often require hydrophobic modification or carbonization, which is often environmentally harmful and energy-intensive. In this study, we introduce a Pickering-emulsion-templating approach to fabricate a cellulose nanofibril (CNF) aerogel with a hierarchical pore structure, allowing for high oil absorption capacity. *n*-Hexane−CNF oil-in-water Pickering emulsions are prepared as an emulsion template, which is further lyophilized to create a hollow microcapsule-based CNF (HM-CNF) aerogel with a density ranging from 1.3 to 6.1 mg/cm^3 and a porosity of ≥99.6%. Scanning electron microscopy and Brunauer−Emmett−Teller analyses reveal the HM-CNF aerogel's hierarchical pore structure, originating from the CNF Pickering emulsion template, and also confirm the aerogel's very high surface area of 216.6 m^2/g with an average pore diameter of 8.6 nm. Furthermore, the aerogel exhibits a maximum absorption capacity of 354 g/g and 166 g/g for chloroform and *n*-hexadecane, respectively, without requiring any surface modification or chemical treatment. These combined findings highlight the potential of the Pickering-emulsion-templated CNF aerogel as an environmentally sustainable and high-performance oil absorbent.

INTRODUCTION

Cellulose nanofibrils (CNF) are a type of nanocellulose with a diameter ranging from 15 to 40 nm and an aspect ratio greater than 50.[1−3] Plant and woody biomass are this fiber-like material's main source of extraction, in which plant and/or wood fibers are first pretreated chemically or enzymatically to ease a defibrillation process and then subjected to a mechanical treatment to produce CNF.[4−6] The unique physicochemical properties of CNF—low density, high aspect ratio, mechanical flexibility, biodegradability, and biocompatibility—have drawn a lot of research attention.[7−9] Thus, a wide range of applications have been proposed for CNF, including composite reinforcement, food packaging, textile dyeing, coatings, thermal insulation, as well as biomedical, electronic, and energy storage devices.[10−16]

An aerogel is a highly porous and low-density material in which a solvent in the gel's network is replaced with a gas without significant shrinkage of the gel network.[17] Aerogels can be made from an array of precursors, such as organic and synthetic polymers, silica, and metal oxides. In particular, nanocellulose-based aerogels, especially using CNF capitalizing on its flexibility and high aspect ratio, have garnered much interest because of their mechanical flexibility, abundance, renewability, biocompatibility, and facile biological degradation.[18−20] CNF-based aerogels feature low density, large porosity, and a high specific surface area that make them suitable for many functional applications, which include biomedical scaffolds, high-capacity absorbents for water treatment, thermal insulation, pressure sensing, and energy storage.[21−24] CNF aerogels can be prepared through several techniques, including supercritical drying,[25] unidirectional or isotropic freeze casting,[26−28] and Pickering emulsion templating.[29,30]

Received: June 1, 2023
Accepted: September 11, 2023
Published: September 25, 2023

© 2023 The Authors. Published by American Chemical Society

A Pickering emulsion is an emulsion stabilized by amphiphilic solid particles that can readily partition at the oil−water interface to reduce surface tension.[31] Compared to conventional surfactants, Pickering emulsions have recently been chosen by many researchers due to their lower toxicity, lower cost, and higher stability against coalescence.[32−34] Instead of surfactants, Pickering emulsions may utilize numerous inorganic particles, including silica, montmorillonite, laponite, calcium carbonate, and carbon graphite.[35] More recently, biobased particles such as cellulose, chitin, chitosan, and starch are being utilized for the formation of Pickering emulsions.[36,37] Nanocelluloses have also been used to create Pickering emulsions, e.g., bacterial nanocellulose (BNC),[38] CNF,[39−43] and cellulose nanocrystals (CNC),[44,45] due to their amphiphilicity, nanoscale size, and low environmental and safety concerns.

When it comes to constructing an aerogel structure, an emulsion-templating method has been reported to fabricate a variety of aerogels.[46−48] This method starts with the preparation of an oil-in-water (O/W) or water-in-oil (W/O) Pickering emulsion. The liquid core (either oil or water) is then removed by sequential solvent exchange or freeze-drying, leaving a hollow microcapsule structure or an associated aerogel structure where the porosity and pore size distribution resemble those of initial emulsion droplets. Specifically, the Pickering-emulsion-templating approach was employed to construct CNF- or CNC-based aerogels with low density and a hierarchical porous structure.[29,30,49−53] Jiménez-Saelices et al. investigated thermal superinsulation properties of CNF-based materials via the structuration of aerogels through the Pickering emulsion templating.[29] In another study by Song et al., a strong, flexible, and super thermal insulating CNF/emulsion composite aerogel with quasi-closed small pores was developed.[30] Due to the unique hierarchical morphology and extremely low density arising from the emulsion template, these emulsion-templated CNF aerogels particularly showed superior thermal insulation performance, whose thermal conductivity was even lower than that of air. Tasset et al. prepared a CNC-based aerogel by freeze-drying O/W emulsions stabilized with CNC. Removal of cyclohexane as an oil phase in this CNC-based O/W Pickering emulsion by lyophilization led to a lightweight cellular foam whose pore size remained similar to the size of emulsion droplets.[51] Considering the lightweight and hierarchical morphology arising from the Pickering emulsion template, the Pickering emulsion-templated aerogels may be useful as a green, high-capacity absorbent. In addition, we note that the Pickering-emulsion-templating approach allowing for the control of the overall porosity and morphology of the resultant aerogel may help improve the absorptive performance of the aerogel. However, there is little knowledge about Pickering emulsion-templated aerogels as an absorbent.

Indeed, many nanocellulose-based aerogels using CNF and BNC have shown excellent oil-absorption performance because of their high porosity, low density, and three-dimensional network featuring interconnected cellulose fibrils.[54,55] Despite their high oil absorption capacity, these nanocellulose-based sorbents are usually prepared by modifying the surface of the aerogel with hydrophobic agents such as alkoxysilanes, chlorosilanes, and metal oxides. The extra hydrophobization step often requires complicated and time-consuming processes, e.g., chemical vapor deposition, atomic layer deposition, and high-temperature carbonization, which would incur negative environmental effects.[22,54,56,57] Moreover, these processes are often energy- and equipment-intensive. Hence, a simple and facile method is desired that enables CNF aerogels to function as a biobased, high-capacity oil absorbent without compromising sustainability.

Herein, we report a Pickering-emulsion-templating method to fabricate a hollow microcapsule-based CNF (HM-CNF) aerogel with a high oil absorption capacity. *n*-Hexane−CNF O/W Pickering emulsions were used as the template for the aerogel. After freeze-drying, which led to the hollow CNF microcapsule-like morphology, the HM-CNF aerogel exhibited low density (1.3 to 6.1 mg/cm^3), high porosity (99.6 to 99.9%), and a hierarchical pore structure arising from the emulsion template, supported by scanning electron microscopy (SEM) and Brunauer−Emmett−Teller (BET) analyses. Without any surface modification of CNF or hydrophobic treatment of an aerogel, the HM-CNF aerogel achieved an ultrahigh oil absorption capacity of 354 g/g for chloroform, demonstrating the potential of the Pickering-emulsion-templating method to produce a biobased, high-capacity oil absorbent.

EXPERIMENTAL SECTION

Materials. Microfibrillated cellulose (Exilva F 01-V) was kindly provided by Borregaard in Norway. *n*-Hexane (95%, Fisher Scientific Co., USA), *n*-hexadecane (99%, Alfa Aesar), chloroform (99.5%, Merck), and Nile red (Chem-Impex International, Inc.) were used without further purification.

Preparation of CNF Suspensions. Microfibrillated cellulose was subjected to a mechanical treatment, and then the resultant slurry was centrifuged to remove large aggregates from nanosized cellulose fibrils. In a typical example, 8.0 g of Exilva microfibrillated cellulose (10 wt % dry CNF in water) was diluted to 0.2 wt % with deionized water. The suspension was then placed in a mechanical blender (Vitamix TNC 5200, Vitamix Corporation, USA) at 22,500 rpm for 5 min. The blending process was closely monitored to prevent overheating of the suspension that may cause thermal degradation of CNF. The resultant aqueous dispersion was then poured into a centrifuge tube and allowed to centrifuge (Beckman Coulter, Avanti 95 JE 14.50 Rotor) at 1500 rpm for 15 min. Supernatant and residue were collected separately, whereby the residue was completely oven-dried at 105 °C for 24 h and its weight was measured to calculate the concentration of CNF in the supernatant. The supernatant was further centrifuged at 9,000 rpm for 15 min to remove excess water.

Characterization of CNF Suspensions. To determine the presence of residual hemicelluloses and lignin in the neat Exilva microfibrillated cellulose, the Fourier transform infrared (FTIR) spectrum of the freeze-dried microfibrillated cellulose (0.1 wt % aqueous suspension) was taken by using a PerkinElmer Spectrum Two spectrophotometer over the range of 400 to 4000 cm^{-1} with a resolution of 0.5 cm^{-1}. Atomic force microscopy (AFM) with a tapping mode (Dimension Icon Bruker, USA) was used to determine the width and length of individual fibrils of CNF. To do so, a single drop of the diluted CNF aqueous suspension (0.001 wt %) was placed on a glass microscope slide and vacuum-dried. AFM scan was performed with a silicon cantilever (Bruker, UK) having a nominal tip radius of 8 nm and a spring constant of 5 N/m with scan areas of 20 × 20 and 5 × 5 μm^2. To determine the level of residual surface charge in CNF, the carboxylic acid content of CNF was estimated by using a conductometric titration method. In a typical example, 50 mL

https://doi.org/10.1021/acsomega.3c03871
ACS Omega 2023, 8, 36856−36867

Scheme 1. Schematic Illustrating the Preparation of a HM-CNF Aerogel Consisting of (1) Mixing of *n*-Hexane and a CNF Suspension in Water, (2) Emulsification by Ultrasonication to Create*n*-Hexane−CNF Pickering Emulsions, and (3) Freeze Drying to Produce the HM-CNF Aerogel

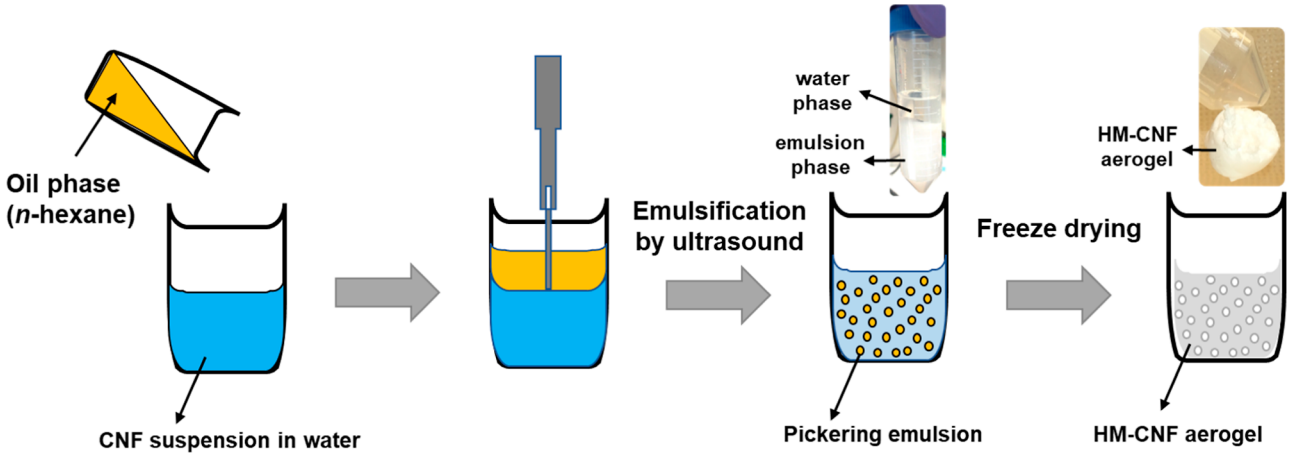

of 0.2 wt % aqueous CNF suspension was mixed with 2 mL of 0.1 M HCl to adjust pH to 3. Then, 1 mL of 50 mM NaCl was added to the solution, and the mixture was stirred prior to titration to enhance the dynamic distribution of ions. The mixture was titrated with 0.1 M NaOH at a rate of 0.1 mL/min. In the titration, the conductivity was measured with a conductometer (Oakton PC2700), and the carboxylate content of CNF was calculated by using eq 1

$$\text{Content of } -\text{COOH (mmol/g)} = C_{\text{NaOH}} \times \frac{(V_2 - V_1)}{m} \tag{1}$$

where C_{NaOH} is the concentration (in mM) of NaOH, V_2 and V_1 (in mL) are the volumes of the NaOH solution determined from a titration curve, and m is the mass of the dry CNF (in g).

Preparation of CNF-Stabilized Pickering Emulsions. O/W Pickering emulsions were made by using *n*-hexane and the CNF aqueous suspension as the oil and water phases, respectively. All of the emulsions were prepared with a water-to-oil ratio of 2:1. In a typical example, 20 mL of an aqueous CNF suspension (0.01−0.5 wt % of dry CNF in water) was topped with 10 mL of *n*-hexane. A probe of the Tekmar Ultrasonic Processor (TM 750, 13 mm probe, 750 W) was placed at the oil−water interface, and ultrasonication was performed at a 50% power level in a 9 s pulse and 1 s standby mode for 5 min. In a minute, the solution became cloudy, indicating the formation of Pickering emulsions. After the ultrasonication, the solution was centrifuged at 2,000 rpm for 3 min, which sped up the formation of a creamy emulsion layer between aqueous (bottom) and oil (top) layers. The middle layer containing the *n*-hexane−CNF emulsions was carefully collected and stored in a sealed container for further analysis.

Characterization of CNF-Stabilized Pickering Emulsions. For an optical microscope analysis, 0.1 mL of the Pickering emulsion and 1 mL of distilled water were mixed by vortex. One drop of the mixture was placed onto a glass microscope slide and observed by a BX51 Olympus microscope under the magnifications of 4× to 20×. Using at least 105 droplet measurements for each sample, the size of the emulsion droplets was estimated by ImageJ software. To visualize the microscopic structure of the emulsion droplets, confocal laser scanning microscopy (CLSM) was used. A stock solution of Nile red (0.1 wt % in *n*-hexane) as a lipophilic fluorescent stain was prepared and used for the synthesis of *n*-hexane-CNF Pickering emulsions, following the same procedure described above. A LSM510 confocal microscope (Zeiss, Gottingen, Germany) was used to acquire CLSM images through a 40× water immersion lens with an optical section thickness of around 2 μm. The excitation wavelength in the CLSM spectra was 543 nm. The surface coverage (C_S) of the CNF-stabilized Pickering emulsions was estimated by the following eq 2.[38,58]

$$C_S = \frac{m_p D}{6h\rho V_{\text{oil}}} \tag{2}$$

where m_p represents the dry mass of CNF particles, D denotes the diameter of the emulsion droplets, h is the thickness of the CNF particles obtained from AFM, ρ represents the density of CNF particles (1.6 g/cm^3),[59] and V_{oil} refers to the volume of *n*-hexane included in the emulsion after centrifugation.

Preparation and Characterization of Hollow Microcapsule-Based CNF Aerogels. Scheme 1 illustrates all of the steps for the preparation of the HM-CNF aerogel. The freshly prepared *n*-hexane-CNF Pickering emulsion was placed in a centrifuge tube, which was initially frozen in liquid nitrogen and then transferred into a freeze-dryer (Labconco FreeZone Plus 4.5 Liter) at −80 °C under 0.018 mbar for 2 days to yield a hollow microcapsule-based CNF (HM-CNF) aerogel.

For investigating the morphology of the as-prepared HM-CNF aerogel with a field emission scanning electron microscope (JSM-129 6500F, JEOL USA) at a 5 kV accelerating voltage, a 5 nm thick platinum layer was sputtered onto the specimen. To determine the density of the HM-CNF aerogel, the diameter and height of the aerogel were measured by a digital caliper, while its weight was determined by using a digital balance. The density, ρ, of the HM-CNF aerogel was calculated according to eq 3

$$\rho = m/v \tag{3}$$

where m and v are the mass and volume of the aerogel, respectively. The porosity, P, of the HM-CNF aerogel was calculated according to eq 4

$$P\ (\%) = \left(1 - \frac{\rho_m}{\rho_c}\right) \times 100 \tag{4}$$

https://doi.org/10.1021/acsomega.3c03871
ACS Omega 2023, 8, 36856−36867

where ρ_m and ρ_c are the density of the aerogel and cellulose (1.6 g/cm^3), respectively.[59] A surface area and porosity analyzer (Autosorb iQ, Quantachrome Instruments) was used to determine the specific surface area and pore size distribution of the aerogel. To measure N_2 adsorption, aerogel samples were degassed at 60 °C under vacuum for 2 h. Based on the linear region of experimental isotherms at 77 K and relative pressures ranging from 0.01 to 0.3, Brunauer–Emmett–Teller (BET) theory was used to calculate the specific surface area of the aerogels. Using the Barrett–Joyner–Halenda (BJH) method, the distribution of the pores in the sample was estimated using the desorption curve of the isotherm. A modified Kelvin equation can be used to relate the removed amount of nitrogen to pore size when relative pressure decreases.[60] Thermogravimetric analysis (TGA, Q600 SDT, TA Instruments) was conducted on a specimen of approximately 10 mg placed in an alumina crucible. With a heating rate of 10 °C/min and a flowing nitrogen atmosphere of 99.99% at 100 mL/min, a thermal scan was conducted from 25 to 600 °C.

Measurement of Oil Absorption Performance of the HM-CNF Aerogel. Prior to the oil absorption test, the initial weight of the HM-CNF aerogel with varying CNF concentrations was measured. Subsequently, the aerogel specimen was completely immersed in *n*-hexane, *n*-hexadecane, cyclohexane, or chloroform until it became fully saturated. Afterward, the aerogel specimen was held on the side of the tube to drain excessive and unabsorbed liquid, and then its weight was taken. The absorption capacity, Q (g/g), was calculated using eq 5

$$Q = \frac{(W_i - W_f)}{W_i} \tag{5}$$

where W_i and W_f are the initial and final weights of the HM-CNF aerogel before and after the oil absorption, respectively. To test the reusability and regeneration of the HM-CNF aerogel, a loaded aerogel sample with *n*-hexane, cyclohexane, or chloroform was distilled at 40 °C under vacuum. The complete evaporation of the absorbed liquid was inferred by the recovery of the initial weight. The retention, R, was determined using eq 6

$$R\ (\%) = \frac{Q_i}{Q_0} \times 100 \tag{6}$$

where Q_0 and Q_i are the initial absorption capacity and the capacity after each recycling cycle of the aerogel. The recycling performance of the aerogel was measured for up to five cycles.

RESULTS AND DISCUSSION

Formation and Characterization of *n*-Hexane–CNF Microcapsules. The FTIR spectrum of the Exilva microfibrillated cellulose (Exilva F 01-V) showed no significant peak at 1738 and 1505 cm^{-1}, indicating most of the lignin and hemicelluloses were removed from the material (see the inset in Figure S1).[61,62] Microfibrillated cellulose was mechanically treated with a blender (Vitamix standard blender), and the diameter and length of the resultant fibers were estimated to be around 40 nm and up to a few tens of micrometers, respectively (see AFM images in Figure S2). These individualized cellulose fibers were reported to be effective in making stable emulsions.[63] The carboxylate content obtained from the conductometric analysis of the aqueous CNF suspension was 0.05 mmol/g (Figure S3). This level of surface charge density may arise from residual carboxylic acid on the surface of cellulose, indicating minimal chemical treatments of Exilva microfibrillated cellulose as our starting material.[64] As a comparison, it was reported that CNC particles with a low sulfate surface charge density (<0.03 charge/nm^2) effectively stabilized O/W Pickering emulsions, while the highly sulfate-charged counterpart did not.[44] Thus, the low charge density on the surface of CNF particles (0.05 mmol/g) in our case is expected to result in reduced electrostatic repulsions between the particles, thereby fostering the stabilization of the CNF particles at the oil–water interface.[33,65]

Optical microscope (OM) images of *n*-hexane–CNF microcapsules are shown in Figure S4. A cloudy and creamy layer showed up within 1 min of ultrasonication, indicating the formation of emulsions. We believe ultrasonication created metastable, spherical oil droplets dispersed in water, which were immediately stabilized by CNF particles, as shown in the OM images of the microcapsules in Figure S4. We also note that the number density of the microcapsules was lower for the emulsions created with ≤0.03% CNF in water (Figure S4a,b) than the other conditions (Figure S4c–i), suggesting two separate types of microcapsule yield. Figure S5 shows the CLSM images of the microcapsules, displaying *n*-hexane dyed in red as the core of the microcapsule. Amphiphilic CNF particles may orient themselves at the oil–water interfaces to lower the surface tension between the oil and water, thereby forming stable O/W emulsions.[66] CNF particles may function as an interfacial stabilizer for the O/W Pickering emulsion because each anhydroglucose unit has polar hydroxyl groups in the equatorial plane while the axial plane is relatively nonpolar, which corresponds to the surfaces of $(1\bar{1}0)$ and (110) cellulose crystal planes, respectively.[67−69]

The average size of the microcapsules and its standard deviation as a function of the CNF concentration are shown in Figure 1. At CNF concentrations ≤0.03%, the microcapsule yield was quite low, indicating the microcapsule formation was not efficient, as shown by the low number density of the microcapsules in Figure S4a,b. For the CNF concentrations of

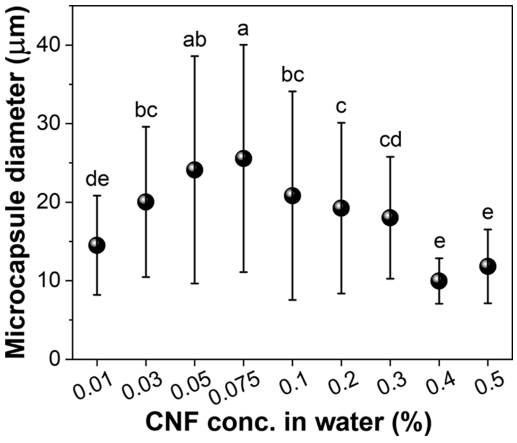

Figure 1. Average size and its standard deviation of *n*-hexane–CNF microcapsules as a function of the CNF concentration in water at the water-to-oil ratio of 2:1. Data were obtained by ImageJ from the OM images partially shown in Figure S4. Letters on top of the individual data points represent statistical grouping ($p < 0.05$) in the mean microcapsule diameter based on one-way analysis of variance (ANOVA) at a 95% confidence interval.

https://doi.org/10.1021/acsomega.3c03871
ACS Omega 2023, 8, 36856−36867

Table 1. Surface Coverage of the *n*-Hexane−CNF Microcapsules with Respect to the Concentration of CNF in Water[a]

CNF concentration (%)	0.01	0.03	0.05	0.075	0.1	0.2	0.3	0.4	0.5
Surface coverage	6%	21%	44%	67%	88%	83%	154%	156%	181%

[a]The water-to-oil ratio was 2:1.

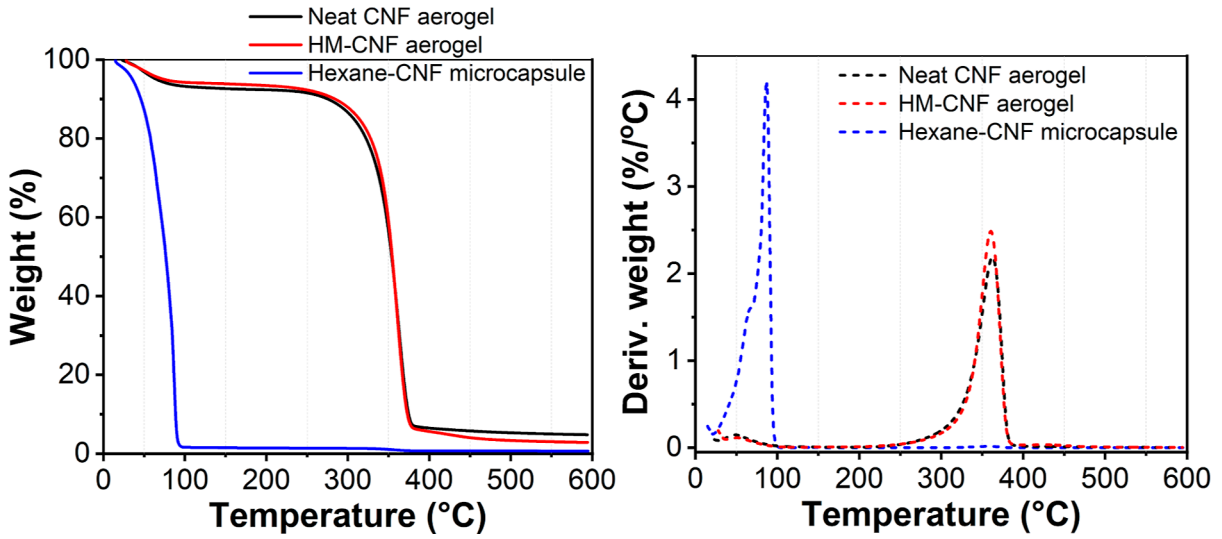

Figure 2. (Left) Weight loss and (right) derivative weight loss profiles of the neat CNF aerogel (in black), the HM-CNF aerogel (in red), and the *n*-hexane−CNF microcapsule (in blue). For both aerogels and the *n*-hexane−CNF microcapsule, the concentration of CNF in water was 0.075%.

0.05, 0.075, and 0.1%, the average microcapsule diameter was similarly around 25 μm, with the surface coverage increasing from 44 to 88% (see Table 1). The similar microcapsule diameter in this range of the CNF concentration may be explained by the balance between the coalescence of metastable O/W emulsions and the stabilization of them by CNF particles, in which only the surface coverage of the microcapsule increased. A similar trend has been reported in BNC-stabilized Pickering emulsions.[38]

At CNF concentrations above 0.1%, the average microcapsule diameter decreased with increasing CNF concentrations. This could be explained by a limited coalescence process whereby the higher the number of particles present in the suspension, the better the stabilization of droplets.[38,43] In other words, as the CNF concentration increases, the irreversible adsorption of CNF particles at the oil−water interface would likely prevent oil droplets from further growing by coalescence. Another reason for the decreased microcapsule diameter could be attributed to the viscosity of the suspension. An increase in the CNF concentration leads to a greater number of CNF particles with an increasing viscosity of the CNF solution, in which steric hindrance caused by CNF particles would further prevent the coalescence of the oil droplets.[43] The limited coalescence process seemed to dominate at the CNF concentration >0.1%, with a smaller standard deviation of the average microcapsule diameter for 0.4 and 0.5% CNF than the other CNF concentrations.

Table 1 displays the estimated surface coverage of the *n*-hexane−CNF microcapsules calculated by eq 2. At a low concentration of CNF up to 0.03%, the surface coverage was even less than 25%. Although stable emulsions with the surface coverage of less than 30% have been reported in the literature,[42,70,71] these microcapsules may suffer limited stability due to a lack of enough CNF particles to fully cover *n*-hexane droplets dispersed in water. When the CNF concentration was from 0.05 to 0.1%, the surface coverage scaled with the CNF concentration, suggesting that the system had enough CNF particles to produce microcapsules with presumably high stability. At this range, the average diameter of the microcapsules remained close to 25 μm with increasing surface coverage. As the CNF concentration became greater than 0.2%, the surface coverage went beyond 100%, which may imply the stacking of extra CNF particles on the surface of the microcapsules or the presence of extra CNF particles connecting individual microcapsules.[43,72]

Thermogravimetric analysis (TGA) was used to characterize the thermal properties of the *n*-hexane−CNF microcapsule and the HM-CNF aerogel. TGA thermograms of the freshly prepared microcapsule in Figure 2 (in blue) show significant weight loss before 100 °C, whose derivative weight loss maximum was at 87 °C with a shoulder peak at around 66 °C. These data indicate the encapsulation of *n*-hexane in the core of the microcapsule. After 100 °C, the remaining weight was less than 2% after water and *n*-hexane evaporated, which is in agreement with the dry weight of CNF in the microcapsule. TGA thermograms of the neat CNF (in black) and the HM-CNF aerogels (in red) were nearly identical, which strongly suggests that the HM-CNF aerogel contained only CNF after the removal of the core *n*-hexane during freeze-drying. Both samples exhibited the weight loss of around 10% up to 250 °C, which was due to the evaporation of bound water to CNF. Thermal degradation and char formation of cellulose in the aerogels occurred between 250 and 400 °C. It is worth noting that the residual weight of the HM-CNF aerogel at 600 °C was slightly lower than that of the neat CNF aerogel. The difference can be attributed to the higher specific surface area of the HM-CNF aerogel, which will be further discussed in the BET analysis. The increased surface area would facilitate the thermal degradation of cellulose, especially considering both aerogels were composed of pure cellulose.

https://doi.org/10.1021/acsomega.3c03871
ACS Omega 2023, 8, 36856−36867

Characterization of the HM-CNF Aerogels. Freshly prepared *n*-hexane-CNF microcapsules were lyophilized to yield the HM-CNF aerogel. Figure 3 shows the density and

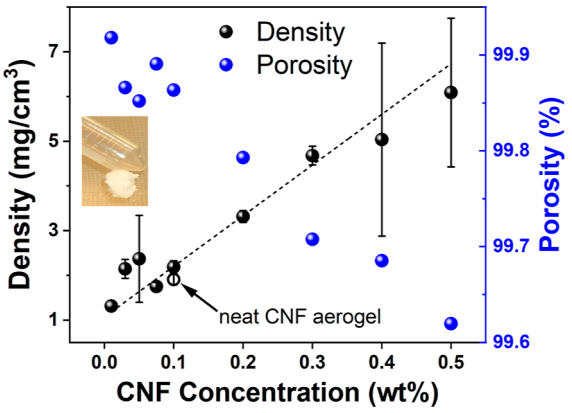

Figure 3. Density and porosity of HM-CNF aerogels as a function of the CNF concentration in water. The standard deviation of density is displayed with an error bar. The density of neat CNF aerogel at 0.1% CNF concentration is also shown as a hollow dot. A dotted line shows the linear fit of the HM-CNF aerogel density as a function of the CNF concentration. The inset photograph shows the 0.3% HM-CNF aerogel being attracted toward a plastic tube by the electrostatic force due to its lightness.

porosity of the HM-CNF and neat CNF aerogels as a function of the CNF concentration in water. The photograph of the HM-CNF aerogel in the inset of Figure 3 demonstrates the lightness of the aerogel. The density of the HM-CNF aerogel increased from 1.3 to 6.1 mg/cm^3, and the porosity decreased from 99.9 to 99.6% with an increasing CNF concentration from 0.01 to 0.5%. Overall, the density of the aerogel scaled with the CNF concentration. The porosity and density of the HM-CNF aerogels are consistent with the values reported in the literature for cellulose-based aerogels, including the density of the 0.1% neat CNF aerogel shown in Figure 3 as a hollow dot.[53,54,73]

Once the core *n*-hexane and the surrounding aqueous phase in the *n*-hexane-CNF O/W Pickering emulsions were removed by lyophilization, a hollow microcapsule-based CNF (HM-CNF) aerogel emerged. Along with the ordinary morphology of a CNF-based aerogel, i.e., individual and entangled CNF, aggregated and/or assembled sheet-like CNF, and interconnected pores,[56,74] the HM-CNF aerogels exhibited a porous, hollow microcapsule-like structure as shown in the SEM images in Figure 4. We note the size of the hollow microcapsules in the aerogel is similar or slightly smaller than that of the *n*-hexane-CNF Pickering emulsion droplets shown in Figures 1, S4 and S5, which is in agreement with other Pickering-emulsion-template-based CNF aerogels.[29,30,51]

At the CNF concentration ≤0.03%, the HM-CNF aerogel appeared to be composed of aggregated CNF with many irregularly shaped, open fibrous structures, whose morphology would likely be inherited from that of *n*-hexane-CNF Pickering emulsions (see Figure 4a for 0.03% HM-CNF). Due to the low surface coverage of the emulsion (see Table 1), it is highly likely that most of the microcapsules were broken during lyophilization, in which the microcapsules would collapse or burst when ice crystals grew during the freezing of water, leading to such porous and irregular morphology.

A microcapsule-like morphology was well preserved for the aerogels at CNF concentrations from 0.05 to 0.1% [Figure 4b−d (low resolution) and h,i (high resolution)], which was possibly due to the high surface coverage, conferring structural integrity to the microcapsules. On the other hand, at the CNF concentration >0.1% (Figure 4e,j), the microcapsule-like morphology in the HM-CNF aerogel was neither obvious nor easily seen. Pickering emulsions stabilized by high-aspect-ratio cellulose nanoparticles such as CNF are known to form a cluster-like structure consisting of Pickering emulsion droplets interconnected to each other by fiber-like cellulose nanoparticles.[42,43,75] Thus, at the high CNF concentration, we believe the majority of hollow microcapsules were embedded and hidden in the matrix of entangled and/or sheet-like CNF, thereby making them obscure.

The microcapsule-like morphology of the HM-CNF aerogel, which resembles that of the Pickering emulsion as the template for the aerogel, with the combination of fiber-like CNF particles interconnecting the microcapsules, created a unique hierarchical pore structure. In particular, the SEM images of 0.075 and 0.1% HM-CNF aerogels (Figure 4c,d and h,i for low- and high-resolution images, respectively) showed that hollow capsule-like globules were loosely connected to each other by individual and entangled CNF particles. Based on the high-resolution SEM images of 0.1% HM-CNF aerogel in Figure S6a−c, we believe there are three different levels of porosity in the HM-CNF aerogels: (1) pores on the surface of the hollow microcapsules (sub-100 nm to a few micrometer), (2) pores from entangled/assembled CNF particles connecting the hollow microcapsules (up to a few micrometers), and (3) pores from the cavity of the hollow microcapsules (bigger than a few micrometers). It should be noted that the microscopic pores arising from the surface and the cavity of the hollow microcapsules were not seen in ordinary CNF aerogels (see Figures 4f,g,k,l and S6g−l), indicating that the mechanism of liquid absorption for the HM-CNF aerogel would be different than that of the ordinary CNF aerogel. Such hierarchical pore structure seemed more prevalent for the HM-CNF aerogels, with the CNF concentration of up to 0.1% than the other aerogels. At the CNF concentration higher than 0.1%, due to overcrowding of CNF particles, the distinction between the first and second levels of porosity—sub-100 nm to a few μm and up to a few μm pores—would become blurred. The overcrowding of CNF particles in the 0.3% HM-CNF aerogel can be seen in Figures 3e,j and S6d−f.

The specific surface area and pore characteristics of HM-CNF and neat CNF aerogels are shown in Figure 5. BET nitrogen adsorption/desorption curves for the 0.1% HM-CNF and neat CNF aerogels in Figure 5a can be classified as mixed type I and type IV isotherms with a clear hysteresis loop, implying adsorption on mesoporous adsorbents exhibiting strong adsorbate−adsorbent interactions.[30,76,77] The HM-CNF aerogel exhibited a steep, almost vertical H1-type hysteresis, indicating a narrow range of uniform mesopores in the aerogel. The shape of the hysteresis loop of the neat CNF aerogel was close to a type H4, which is often associated with narrow slit-like pores, indicating that the pore network consists of nonrigid aggregates of plate-like particles with some macropores that are not entirely filled with pore condensate.[78]

Table 2 summarizes the BET specific surface area (SSA) and average pore diameter of 0.1% HM-CNF and neat 0.1% CNF aerogels, which were estimated by using the BET nitrogen adsorption/desorption isotherms in Figure 5a. The surface area

https://doi.org/10.1021/acsomega.3c03871
ACS Omega 2023, 8, 36856−36867

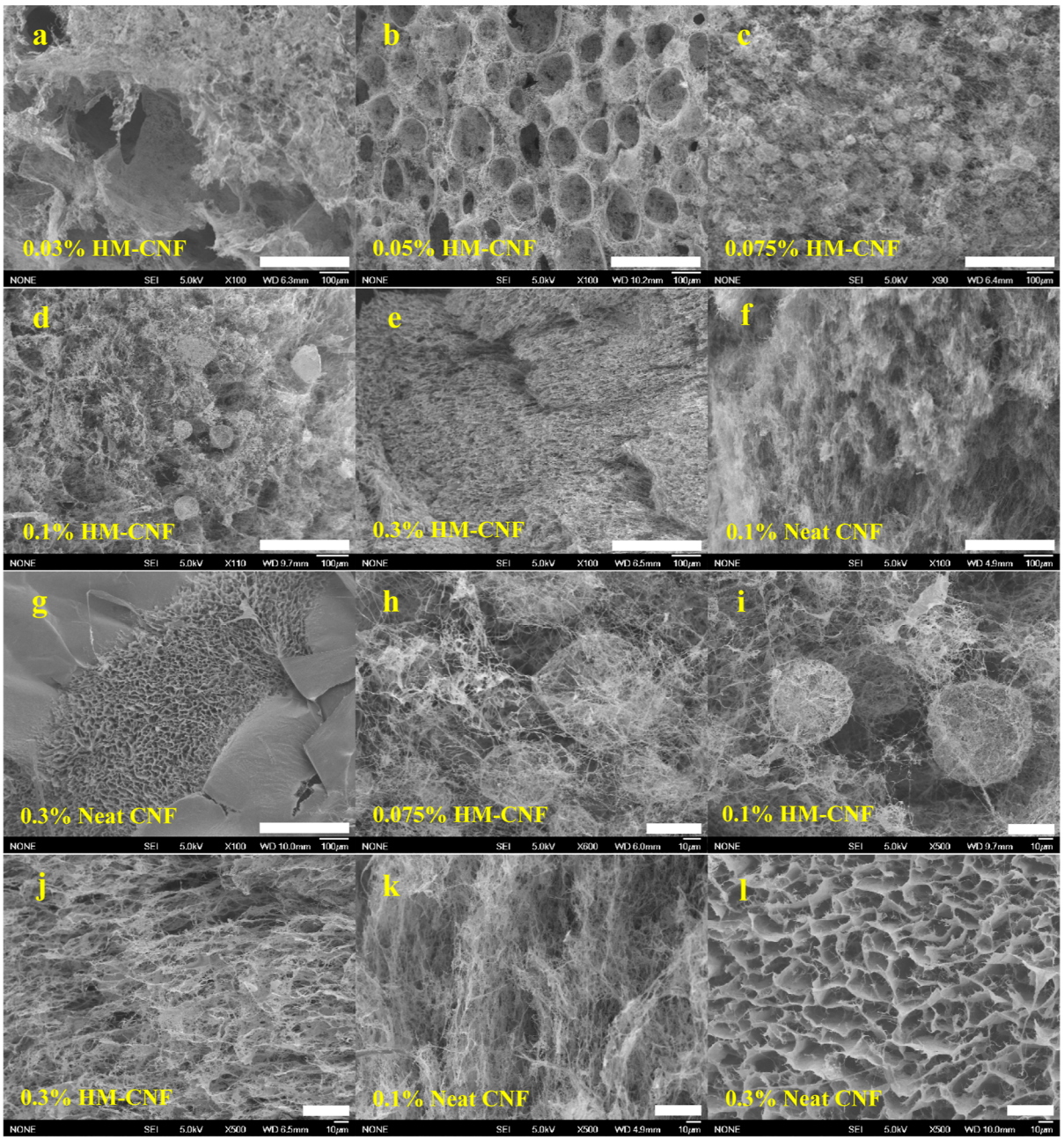

Figure 4. SEM images of the HM-CNF aerogels with the CNF concentrations of (a) 0.03, (b) 0.05, (c) 0.075, (d) 0.1, and (e) 0.3%. Neat CNF aerogels with the CNF concentrations of (f) 0.1, (g) 0.3%. High-resolution images for the HM-CNF aerogels: (h) 0.075, (i) 0.1, and (j) 0.3%. High-resolution images for the neat CNF aerogels: (k) 0.1 and (l) 0.3%. 300 μm scale bars for (a−g) and 30 μm for (h−l).

of the neat CNF aerogel (37.0 m^2/g) falls within the range of SSA values from CNF aerogels without any surface modification or solvent exchange in the literature.[54] It has been reported that during the freeze-drying of a CNF hydrogel, water becomes ice crystals that nucleate and grow in a way that CNF located in between the ice crystals will self-assemble, which leads to a formation of thin cell walls made of the assembled CNF.[56,79] Such a characteristic morphology of CNF aerogels is clearly seen in Figures 4l and S5j−l. In contrast, the SSA of the 0.1% HM-CNF aerogel (216.6 m^2/g) was 5.9 times higher than that of the neat CNF aerogel, which can be attributed to the hierarchical morphology of the HM-CNF aerogel arising from the Pickering emulsion template. We note that the HM-CNF aerogel in this study marks one of the highest SSAs from CNF-based aerogels to the best of our knowledge.[54]

Although the BJH model has been widely employed to estimate the pore size distribution of CNF aerogels, there is a clear limitation of the method, assuming all pores are rigid and of a regular shape, which may not always hold true.[76,77] With that in mind, we used this model to compare the differences in the average pore diameter between the HM-CNF and neat CNF aerogels. As shown in Table 2, the average pore diameter of the 0.1% HM-CNF aerogel (8.6 nm) was much smaller than the neat CNF aerogel (30.0 nm). As discussed earlier with the SEM images in Figure 4h,i, the hierarchical pore structure of the HM-CNF aerogels, arising from the Pickering emulsion template, may lead to the smaller average pore diameter.

https://doi.org/10.1021/acsomega.3c03871
ACS Omega 2023, 8, 36856−36867

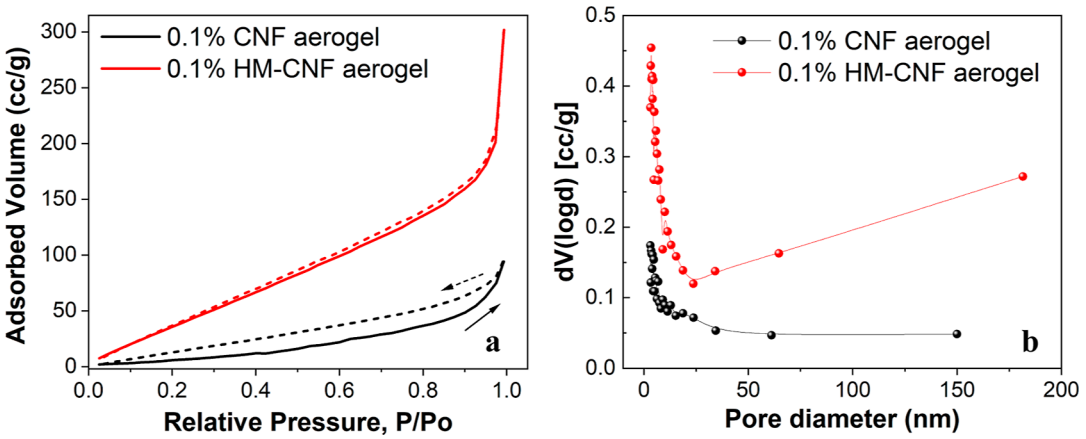

Figure 5. (a) N_2 adsorption/desorption isotherms and (b) pore diameter distributions of neat CNF (0.1%) and HM-CNF (0.1%) aerogels.

Table 2. BET Specific Surface Area and Average Pore Diameter of the HM-CNF and Neat CNF Aerogels

Aerogel type	BET specific surface area (m^2/g)	Average pore diameter (nm)
HM-CNF, 0.1%	216.6	8.6
Neat CNF, 0.1%	37.0	30.0

However, we note that these estimates are based on geometrical assumptions. In addition, it is very likely that large pores are not included in our N_2 adsorption measurements. Overall, the notable differences in SSA and the average pore diameter suggest the overall micropore structure of the HM-CNF aerogel was substantially different from that of the neat CNF aerogel.

Oil Absorption Performance of HM-CNF Aerogels. To examine the potential of the HM-CNF aerogels as an oil absorbent, the absorption capacity of the aerogels against chloroform and *n*-hexadecane, whose densities are 1.49 and 0.77 g/cm^3, respectively, was investigated. During the test, the HM-CNF aerogels from the CNF concentration of 0.01 to 0.5% were compared with the neat CNF aerogels (0.1 and 0.3%). The absorption capacity results in Figure 6a show that all of the HM-CNF aerogels outperformed the neat CNF aerogel except for the 0.01% HM-CNF, in which the microcapsule yield was very low due to the low surface coverage (see Table 1). In addition, 0.03% HM-CNF aerogel exhibited the largest standard deviation, which can be attributed to the low surface coverage of the emulsion template and associated instability of the resultant aerogel. The absorption capacity for chloroform was very high for 0.03 to 0.1% HM-CNF aerogels, particularly reaching 354 g/g for 0.05% HM-CNF, which makes the HM-CNF aerogel as one of the best-performing biobased oil absorbents to the best of our knowledge (see Table S1 for comparison).[54,55] The maximum absorption capacity of the HM-CNF aerogel for chloroform was 2.6 times higher than that of the neat 0.1% CNF aerogel (138 g/g). The absorption capacity for chloroform significantly decreased for the HM-CNF aerogels when the CNF concentration went beyond 0.1%, with gradually reduced capacity as the concentration rose. However, the absorption capacity of 0.3% HM-CNF aerogel, 161 g/g for chloroform, still surpassed that of neat CNF aerogels (106 g/g for 0.3% CNF, data not shown in Figure 6a). It should be noted that most of the high-performance nanocellulose-based aerogels require TEMPO oxidation and/or surface modifications of the aerogels to maximize the oil absorption capacity. In contrast, our HM-CNF aerogel is not involved with any extensive chemical modification of cellulose particles or the hydrophobization of an aerogel, which makes our approach unique and sustainable.

Absorption capacity for *n*-hexadecane also followed the same trend to chloroform, in which 0.03 to 0.1% HM-CNF aerogels marked the highest performance, yielding a maximum absorption capacity of 166 g/g for 0.05% HM-CNF aerogel. There was a reduction in absorption capacity at the higher CNF concentration ≥0.1%, which was the same case to chloroform. We note that the ratio of maximum absorption

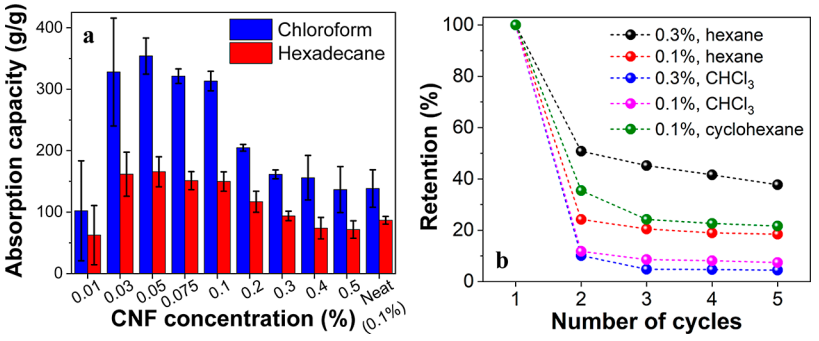

Figure 6. (a) Absorption capacity (g/g) and its standard deviation of the HM-CNF and neat CNF (0.1%) aerogels to chloroform and *n*-hexadecane at the various CNF concentrations. (b) Retention of absorption capacity of the HM-CNF aerogels (0.1−0.3%) up to 5 cycles of absorption−distillation of *n*-hexane, chloroform, and cyclohexane.

https://doi.org/10.1021/acsomega.3c03871
ACS Omega 2023, 8, 36856−36867

capacity (354 g/g for chloroform to 166 g/g for *n*-hexadecane) remained close to the density ratio of the two liquids.

The superior oil absorption performance of the HM-CNF aerogel can be attributed to its hollow microcapsule-like hierarchical morphology that brought about a high SSA (216.6 m^2/g). In addition, we note that the HM-CNF aerogel was fabricated from the O/W Pickering emulsion template, conferring hydrophilic and hydrophobic surface properties to the outer and inner parts of the hollow microcapsule, respectively. Although these microcapsules are connected to each other by amphiphilic CNF particles, as shown in Figure 4h,i, the overall surface property of the HM-CNF aerogel is expected to be different from that of a neat CNF aerogel. In fact, as shown in Video S1, the absorption of red-dyed mineral oil on the surface of 0.1% HM-CNF aerogel was slower than that of 0.1% CNF aerogel, suggesting less hydrophobic HM-CNF aerogel than neat CNF aerogel. The absorption speed of water appeared to be the same for both aerogels (Video S2).

The absorption capacity of the HM-CNF aerogels (0.1 to 0.3%) for *n*-hexane, cyclohexane, or chloroform up to five cycles of absorption−distillation is shown in Figure 6b. All of the HM-CNF aerogels displayed a substantial reduction in retention in the second cycle, followed by rather marginal capacity loss in the following cycles up to 5, as shown in Figure S7a for 0.1% HM-CNF aerogel with *n*-hexane. Neat CNF aerogels exhibited the same trend (Figure S7b). The higher the density of the HM-CNF aerogel, the higher the retention of absorption capacity. For *n*-hexane, the highest retention of 38% after 5 cycles came from the 0.3% HM-CNF aerogel. We suspect the HM-CNF aerogel may undergo structural deformation after the first cycle, possibly due to the collapse of pores, which would reduce the pore volume of the aerogel. Thus, the lowered pore volume of the aerogel led to lower absorption capacity.[80] Since absorption capacity after the second cycle did not reduce significantly, we believe no further structural deformation occurred.

CONCLUSIONS

A Pickering emulsion-templating method was used to create a CNF-based aerogel featuring a hierarchical pore structure with an ultrahigh oil absorption capacity. *n*-Hexane-CNF O/W Pickering emulsions with a CNF concentration from 0.01 to 0.5% were prepared and used as the emulsion template for the aerogel. Lyophilization of the emulsions resulted in the hollow microcapsule-based CNF (HM-CNF) aerogel with a density of 1.3−6.1 mg/cm^3 and porosity of ≥99.6%. SEM investigation revealed the unique hierarchical pore structure of the aerogel arising from the emulsion template, which was believed to lead to a very high BET surface area of 216.6 m^2/g with an average pore diameter of 8.6 nm. Because of the hierarchical pore structure, the HM-CNF aerogel obtained the maximum absorption capacity of 354 and 166 g/g for chloroform and *n*-hexadecane, respectively, without any surface modification or chemical treatment. Due to the O/W Pickering emulsion-dictated surface property, the HM-CNF aerogel was overall less hydrophobic than the neat CNF aerogel, which was confirmed by the slower absorption of hydrophobic mineral oil. Probably due to the low density of the HM-CNF aerogel, the retention of absorption capacity remained less than 40% after five cycles of absorption−distillation. Combined data suggest the potential of the CNF Pickering emulsion-templated aerogel as a biobased, high-capacity oil absorbent without the need for an extra hydrophobization process.

ASSOCIATED CONTENT

Supporting Information

The Supporting Information is available free of charge at https://pubs.acs.org/doi/10.1021/acsomega.3c03871.

FTIR spectrum of neat Exilva microfibrillated cellulose; tapping-mode AFM height images of AFM images of mechanically blended microfibrillated cellulose fibers; curve showing the conductometric titrations of unmodified CNFs; optical microscopy images of *n*-hexane-CNF microcapsules and confocal laser scanning micrographs of *n*-hexane-CNF microcapsules; SEM images of HM-CNF and neat CNF aerogels, absorption capacity of the 0.1% HM-CNF aerogel upon absorption and distillation of *n*-hexane up to five cycles, and the retention of absorption capacity of the neat CNF aerogels up to 5 cycles of absorption−distillation of *n*-hexane and chloroform; and BET specific area and maximum absorption capacity of aerogel-based oil sorbents derived from nanocelluloses (PDF)

HM-CNF and neat CNF aerogels absorbing water (dyed in blue) and mineral oil (dyed in red) (MP4)

(MP4)

AUTHOR INFORMATION

Corresponding Author

Yunsang Kim − *Department of Sustainable Bioproducts, Mississippi State University, Starkville, Mississippi 39759, United States;* orcid.org/0000-0002-5330-1670; Email: yunsang.kim@msstate.edu

Authors

Shuaib A. Mubarak − *Department of Sustainable Bioproducts, Mississippi State University, Starkville, Mississippi 39759, United States;* orcid.org/0000-0002-4068-158X

Islam Elsayed − *Department of Sustainable Bioproducts, Mississippi State University, Starkville, Mississippi 39759, United States*

El Barbary Hassan − *Department of Sustainable Bioproducts, Mississippi State University, Starkville, Mississippi 39759, United States;* orcid.org/0000-0002-7980-9800

Complete contact information is available at: https://pubs.acs.org/10.1021/acsomega.3c03871

Notes

The authors declare no competing financial interest.

ACKNOWLEDGMENTS

The authors wish to acknowledge the support of the U.S. Department of Agriculture (USDA), Research, Education, and Economics (REE), Agriculture Research Service (ARS), Administrative and Financial Management (AFM), Financial Management and Accounting Division (FMAD) Grants and Agreements Management Branch (GAMB), under agreement no. 58-0204-0-098 and 58-0204-1-178. This material is based upon work that supported by the National Institute of Food and Agriculture, U.S. Department of Agriculture, under award number 2021-67022-34003. This publication is a contribution of the Forest and Wildlife Research Center, Mississippi State University. The authors wish to thank Dr. Jason Street in the Department of Sustainable Bioproducts at Mississippi State University for allowing the use of the high-power ultrasonic processor.

REFERENCES

(1) Klemm, D.; Heublein, B.; Fink, H.-P.; Bohn, A. Cellulose: Fascinating Biopolymer and Sustainable Raw Material. *Angew. Chem., Int. Ed.* **2005**, *44* (22), 3358−3393.

(2) Zhao, J.; He, X.; Wang, Y.; Zhang, W.; Zhang, X.; Zhang, X.; Deng, Y.; Lu, C. Reinforcement of all-cellulose nanocomposite films using native cellulose nanofibrils. *Carbohydr. Polym.* **2014**, *104*, 143−150.

(3) Kriechbaum, K.; Munier, P.; Apostolopoulou-Kalkavoura, V.; Lavoine, N. Analysis of the Porous Architecture and Properties of Anisotropic Nanocellulose Foams: A Novel Approach to Assess the Quality of Cellulose Nanofibrils (CNFs). *ACS Sustainable Chem. Eng.* **2018**, *6* (9), 11959−11967.

(4) Abdul Khalil, H. P. S.; Davoudpour, Y.; Islam, M. N.; Mustapha, A.; Sudesh, K.; Dungani, R.; Jawaid, M. Production and modification of nanofibrillated cellulose using various mechanical processes: A review. *Carbohydr. Polym.* **2014**, *99*, 649−665.

(5) Wang, L.; Li, K.; Copenhaver, K.; Mackay, S.; Lamm, M. E.; Zhao, X.; Dixon, B.; Wang, J.; Han, Y.; Neivandt, D.; Johnson, D. A.; Walker, C. C.; Ozcan, S.; Gardner, D. J. Review on Nonconventional Fibrillation Methods of Producing Cellulose Nanofibrils and Their Applications. *Biomacromolecules* **2021**, *22* (10), 4037−4059.

(6) Kim, Y.; McCoy, L. T.; Feit, C.; Mubarak, S. A.; Sharma, S.; Minko, S. Carboxymethyl Cellulose Enhanced Production of Cellulose Nanofibrils. *Fibers* **2021**, *9* (9), 57.

(7) Klemm, D.; Kramer, F.; Moritz, S.; Lindström, T.; Ankerfors, M.; Gray, D.; Dorris, A. Nanocelluloses: A New Family of Nature-Based Materials. *Angew. Chem., Int. Ed.* **2011**, *50* (24), 5438−5466.

(8) *Nanocellulose: from fundamentals to advanced materials*; Wiley-VCH: Weinheim, 2019; p 486.

(9) Patil, T. V.; Patel, D. K.; Dutta, S. D.; Ganguly, K.; Santra, T. S.; Lim, K.-T. Nanocellulose, a versatile platform: From the delivery of active molecules to tissue engineering applications. *Bioact. Mater.* **2022**, *9*, 566−589.

(10) Kim, Y.; McCoy, L. T.; Lee, E.; Lee, H.; Saremi, R.; Feit, C.; Hardin, I. R.; Sharma, S.; Mani, S.; Minko, S. Environmentally sound textile dyeing technology with nanofibrillated cellulose. *Green Chem.* **2017**, *19*, 4031−4035.

(11) Klemm, D.; Cranston, E. D.; Fischer, D.; Gama, M.; Kedzior, S. A.; Kralisch, D.; Kramer, F.; Kondo, T.; Lindström, T.; Nietzsche, S.; Petzold-Welcke, K.; Rauchfuß, F. Nanocellulose as a natural source for groundbreaking applications in materials science: Today's state. *Mater. Today* **2018**, *21* (7), 720−748.

(12) Trache, D.; Tarchoun, A. F.; Derradji, M.; Hamidon, T. S.; Masruchin, N.; Brosse, N.; Hussin, M. H. Nanocellulose: From Fundamentals to Advanced Applications. *Front. Chem.* **2020**, *8*, 392.

(13) Isogai, A. Emerging Nanocellulose Technologies: Recent Developments. *Adv. Mater.* **2021**, *33* (28), 2000630.

(14) Eichhorn, S. J.; Etale, A.; Wang, J.; Berglund, L. A.; Li, Y.; Cai, Y.; Chen, C.; Cranston, E. D.; Johns, M. A.; Fang, Z.; Li, G.; Hu, L.; Khandelwal, M.; Lee, K. Y.; Oksman, K.; Pinitsoontorn, S.; Quero, F.; Sebastian, A.; Titirici, M. M.; Xu, Z.; Vignolini, S.; Frka-Petesic, B. Current international research into cellulose as a functional nanomaterial for advanced applications. *J. Mater. Sci.* **2022**, *57* (10), 5697−5767.

(15) Xiao, J.; Li, H.; Zhang, H.; He, S.; Zhang, Q.; Liu, K.; Jiang, S.; Duan, G.; Zhang, K. Nanocellulose and its derived composite electrodes toward supercapacitors: Fabrication, properties, and challenges. *J. Bioresour. Bioprod.* **2022**, *7* (4), 245−269.

(16) Chen, Y.; Luo, H.; Guo, H.; Liu, K.; Mei, C.; Li, Y.; Duan, G.; He, S.; Han, J.; Zheng, J.; E, S.; Jiang, S. Anisotropic cellulose nanofibril composite sponges for electromagnetic interference shielding with low reflection loss. *Carbohydr. Polym.* **2022**, *276*, 118799.

(17) Pereira, A. L. S.; Feitosa, J. P. A.; Morais, J. P. S.; Rosa, M. d. F. Bacterial cellulose aerogels: Influence of oxidation and silanization on mechanical and absorption properties. *Carbohydr. Polym.* **2020**, *250*, 116927.

(18) Lavoine, N.; Bergström, L. Nanocellulose-based foams and aerogels: processing, properties, and applications. *J. Mater. Chem. A* **2017**, *5* (31), 16105−16117.

(19) Ahankari, S.; Paliwal, P.; Subhedar, A.; Kargarzadeh, H. Recent Developments in Nanocellulose-Based Aerogels in Thermal Applications: A Review. *ACS Nano* **2021**, *15* (3), 3849−3874.

(20) Chhetri, K.; Subedi, S.; Muthurasu, A.; Ko, T. H.; Dahal, B.; Kim, H. Y. A review on nanofiber reinforced aerogels for energy storage and conversion applications. *J. Energy Storage* **2022**, *46*, 103927.

(21) Zaman, A.; Huang, F.; Jiang, M.; Wei, W.; Zhou, Z. Preparation, Properties, and Applications of Natural Cellulosic Aerogels: A Review. *Energy Built Environ.* **2020**, *1* (1), 60−76.

(22) Chen, Y.; Zhang, L.; Yang, Y.; Pang, B.; Xu, W.; Duan, G.; Jiang, S.; Zhang, K. Recent Progress on Nanocellulose Aerogels: Preparation, Modification, Composite Fabrication, Applications. *Adv. Mater.* **2021**, *33* (11), 2005569.

(23) Ji, F.; Sun, Z.; Hang, T.; Zheng, J.; Li, X.; Duan, G.; Zhang, C.; Chen, Y. Flexible piezoresistive pressure sensors based on nanocellulose aerogels for human motion monitoring: A review. *Compos. Commun.* **2022**, *35*, 101351.

(24) Chen, Y.; Hanshe, M.; Sun, Z.; Zhou, Y.; Mei, C.; Duan, G.; Zheng, J.; E, S.; Jiang, S. Lightweight and anisotropic cellulose nanofibril/rectorite composite sponges for efficient dye adsorption and selective separation. *Int. J. Biol. Macromol.* **2022**, *207*, 130−139.

(25) Kobayashi, Y.; Saito, T.; Isogai, A. Aerogels with 3D Ordered Nanofiber Skeletons of Liquid-Crystalline Nanocellulose Derivatives as Tough and Transparent Insulators. *Angew. Chem.* **2014**, *126* (39), 10562−10565.

(26) Scotti, K. L.; Dunand, D. C. Freeze casting - A review of processing, microstructure and properties via the open data repository, FreezeCasting.net. *Prog. Mater. Sci.* **2018**, *94*, 243−305.

(27) Zhang, X.; Liu, M.; Wang, H.; Yan, N.; Cai, Z.; Yu, Y. Ultralight, hydrophobic, anisotropic bamboo-derived cellulose nanofibrils aerogels with excellent shape recovery via freeze-casting. *Carbohydr. Polym.* **2019**, *208*, 232−240.

(28) Chen, Y.; Li, S.; Li, X.; Mei, C.; Zheng, J.; E, S.; Duan, G.; Liu, K.; Jiang, S. Liquid Transport and Real-Time Dye Purification via Lotus Petiole-Inspired Long-Range-Ordered Anisotropic Cellulose Nanofibril Aerogels. *ACS Nano* **2021**, *15* (12), 20666−20677.

(29) Jiménez-Saelices, C.; Seantier, B.; Grohens, Y.; Capron, I. Thermal Superinsulating Materials Made from Nanofibrillated Cellulose-Stabilized Pickering Emulsions. *ACS Appl. Mater. Interfaces* **2018**, *10* (18), 16193−16202.

(30) Song, M.; Jiang, J.; Qin, H.; Ren, X.; Jiang, F. Flexible and Super Thermal Insulating Cellulose Nanofibril/Emulsion Composite Aerogel with Quasi-Closed Pores. *ACS Appl. Mater. Interfaces* **2020**, *12* (40), 45363−45372.

(31) Low, L. E.; Siva, S. P.; Ho, Y. K.; Chan, E. S.; Tey, B. T. Recent advances of characterization techniques for the formation, physical properties and stability of Pickering emulsion. *Adv. Colloid Interface Sci.* **2020**, *277*, 102117.

(32) Briggs, N.; Raman, A. K. Y.; Barrett, L.; Brown, C.; Li, B.; Leavitt, D.; Aichele, C. P.; Crossley, S. Stable pickering emulsions using multi-walled carbon nanotubes of varying wettability. *Colloids Surf., A* **2018**, *537*, 227−235.

(33) Tang, C.; Chen, Y.; Luo, J.; Low, M. Y.; Shi, Z.; Tang, J.; Zhang, Z.; Peng, B.; Tam, K. C. Pickering emulsions stabilized by hydrophobically modified nanocellulose containing various structural characteristics. *Cellulose* **2019**, *26* (13−14), 7753−7767.

(34) Jiang, H.; Sheng, Y.; Ngai, T. Pickering emulsions: Versatility of colloidal particles and recent applications. *Curr. Opin. Colloid Interface Sci.* **2020**, *49*, 1−15.

(35) Chevalier, Y.; Bolzinger, M.-A. Emulsions stabilized with solid nanoparticles: Pickering emulsions. *Colloids Surf., A* **2013**, *439*, 23−34.

(36) Gonzalez Ortiz, D.; Pochat-Bohatier, C.; Cambedouzou, J.; Bechelany, M.; Miele, P. Current Trends in Pickering Emulsions:

https://doi.org/10.1021/acsomega.3c03871
ACS Omega 2023, 8, 36856−36867

Particle Morphology and Applications. *Engineering* **2020**, *6* (4), 468−482.
(37) Pang, B.; Liu, H.; Zhang, K. Recent progress on Pickering emulsions stabilized by polysaccharides-based micro/nanoparticles. *Adv. Colloid Interface Sci.* **2021**, *296*, 102522.
(38) Kalashnikova, I.; Bizot, H.; Cathala, B.; Capron, I. New Pickering Emulsions Stabilized by Bacterial Cellulose Nanocrystals. *Langmuir* **2011**, *27* (12), 7471−7479.
(39) Xhanari, K.; Syverud, K.; Chinga-Carrasco, G.; Paso, K.; Stenius, P. Structure of nanofibrillated cellulose layers at the o/w interface. *J. Colloid Interface Sci.* **2011**, *356* (1), 58−62.
(40) Gestranius, M.; Stenius, P.; Kontturi, E.; Sjöblom, J.; Tammelin, T. Phase behaviour and droplet size of oil-in-water Pickering emulsions stabilised with plant-derived nanocellulosic materials. *Colloids Surf., A* **2017**, *519*, 60−70.
(41) Thompson, K. L.; Derry, M. J.; Hatton, F. L.; Armes, S. P. Long-Term Stability of n-Alkane-in-Water Pickering Nanoemulsions: Effect of Aqueous Solubility of Droplet Phase on Ostwald Ripening. *Langmuir* **2018**, *34* (31), 9289−9297.
(42) Lu, Y.; Li, J.; Ge, L.; Xie, W.; Wu, D. Pickering emulsion stabilized with fibrous nanocelluloses: Insight into fiber flexibility-emulsifying capacity relations. *Carbohydr. Polym.* **2021**, *255*, 117483.
(43) Bahsi Kaya, G.; Kim, Y.; Callahan, K.; Kundu, S. Micro-encapsulated phase change material via Pickering emulsion stabilized by cellulose nanofibrils for thermal energy storage. *Carbohydr. Polym.* **2022**, *276*, 118745.
(44) Kalashnikova, I.; Bizot, H.; Cathala, B.; Capron, I. Modulation of Cellulose Nanocrystals Amphiphilic Properties to Stabilize Oil/Water Interface. *Biomacromolecules* **2012**, *13* (1), 267−275.
(45) Fujisawa, S.; Togawa, E.; Kuroda, K. Nanocellulose-stabilized Pickering emulsions and their applications. *Sci. Technol. Adv. Mater.* **2017**, *18* (1), 959−971.
(46) Teo, N.; Jana, S. C. Open Cell Aerogel Foams via Emulsion Templating. *Langmuir* **2017**, *33* (44), 12729−12738.
(47) Teo, N.; Gu, Z.; Jana, S. C. Polyimide-based aerogel foams, via emulsion-templating. *Polymer* **2018**, *157*, 95−102.
(48) Mawhinney, K.; Jana, S. C. Design Of Emulsion-Templated Mesoporous-Macroporous Polyurea Gels and Aerogels. *ACS Appl. Polym. Mater.* **2019**, *1* (11), 3115−3129.
(49) Cervin, N. T.; Andersson, L.; Ng, J. B. S.; Olin, P.; Bergström, L.; Wågberg, L. Lightweight and Strong Cellulose Materials Made from Aqueous Foams Stabilized by Nanofibrillated Cellulose. *Biomacromolecules* **2013**, *14* (2), 503−511.
(50) Nypelö, T.; Rodriguez-Abreu, C.; Kolen'ko, Y. V.; Rivas, J.; Rojas, O. J. Microbeads and Hollow Microcapsules Obtained by Self-Assembly of Pickering Magneto-Responsive Cellulose Nanocrystals. *ACS Appl. Mater. Interfaces* **2014**, *6* (19), 16851−16858.
(51) Tasset, S.; Cathala, B.; Bizot, H.; Capron, I. Versatile cellular foams derived from CNC-stabilized Pickering emulsions. *RSC Adv.* **2014**, *4* (2), 893−898.
(52) Bago Rodriguez, A. M.; Binks, B. P. Capsules from Pickering emulsion templates. *Curr. Opin. Colloid Interface Sci.* **2019**, *44*, 107−129.
(53) Qiao, M.; Yang, X.; Zhu, Y.; Guerin, G.; Zhang, S. Ultralight Aerogels with Hierarchical Porous Structures Prepared from Cellulose Nanocrystal Stabilized Pickering High Internal Phase Emulsions. *Langmuir* **2020**, *36* (23), 6421−6428.
(54) Liu, H.; Geng, B.; Chen, Y.; Wang, H. Review on the Aerogel-Type Oil Sorbents Derived from Nanocellulose. *ACS Sustainable Chem. Eng.* **2017**, *5* (1), 49−66.
(55) Doshi, B.; Sillanpää, M.; Kalliola, S. A review of bio-based materials for oil spill treatment. *Water Res.* **2018**, *135*, 262−277.
(56) Jiang, F.; Hsieh, Y.-L. Amphiphilic superabsorbent cellulose nanofibril aerogels. *J. Mater. Chem. A* **2014**, *2* (18), 6337−6342.
(57) Zanini, M.; Lavoratti, A.; Lazzari, L. K.; Galiotto, D.; Pagnocelli, M.; Baldasso, C.; Zattera, A. J. Producing aerogels from silanized cellulose nanofiber suspension. *Cellulose* **2017**, *24* (2), 769−779.
(58) Gautier, F.; Destribats, M.; Perrier-Cornet, R.; Dechézelles, J. F.; Giermanska, J.; Héroguez, V.; Ravaine, S.; Leal-Calderon, F.; Schmitt, V. Pickering emulsions with stimulable particles: from highly- to weakly-covered interfaces. *Phys. Chem. Chem. Phys.* **2007**, *9* (48), 6455−6462.
(59) Daicho, K.; Kobayashi, K.; Fujisawa, S.; Saito, T. Crystallinity-Independent yet Modification-Dependent True Density of Nanocellulose. *Biomacromolecules* **2020**, *21* (2), 939−945.
(60) Barrett, E. P.; Joyner, L. G.; Halenda, P. P. The Determination of Pore Volume and Area Distributions in Porous Substances. I. Computations from Nitrogen Isotherms. *J. Am. Chem. Soc.* **1951**, *73* (1), 373−380.
(61) Sain, M.; Panthapulakkal, S. Bioprocess preparation of wheat straw fibers and their characterization. *Ind. Crops Prod.* **2006**, *23* (1), 1−8.
(62) Chen, W.; Yu, H.; Liu, Y.; Hai, Y.; Zhang, M.; Chen, P. Isolation and characterization of cellulose nanofibers from four plant cellulose fibers using a chemical-ultrasonic process. *Cellulose* **2011**, *18* (2), 433−442.
(63) Winuprasith, T.; Suphantharika, M. Microfibrillated cellulose from mangosteen (Garcinia mangostana L.) rind: Preparation, characterization, and evaluation as an emulsion stabilizer. *Food Hydrocolloids* **2013**, *32* (2), 383−394.
(64) Foster, E. J.; Moon, R. J.; Agarwal, U. P.; Bortner, M. J.; Bras, J.; Camarero-Espinosa, S.; Chan, K. J.; Clift, M. J. D.; Cranston, E. D.; Eichhorn, S. J.; Fox, D. M.; Hamad, W. Y.; Heux, L.; Jean, B.; Korey, M.; Nieh, W.; Ong, K. J.; Reid, M. S.; Renneckar, S.; Roberts, R.; Shatkin, J. A.; Simonsen, J.; Stinson-Bagby, K.; Wanasekara, N.; Youngblood, J. Current characterization methods for cellulose nanomaterials. *Chem. Soc. Rev.* **2018**, *47* (8), 2609−2679.
(65) Goi, Y.; Fujisawa, S.; Saito, T.; Yamane, K.; Kuroda, K.; Isogai, A. Dual Functions of TEMPO-Oxidized Cellulose Nanofibers in Oil-in-Water Emulsions: A Pickering Emulsifier and a Unique Dispersion Stabilizer. *Langmuir* **2019**, *35* (33), 10920−10926.
(66) Yao, C.; Shi, G.; Hu, Y.; Zhuo, H.; Chen, Z.; Peng, X.; Zhong, L.; Liu, C. Emulsion templated advanced functional materials from emerging nano building blocks. *J. Mater. Chem. A* **2021**, *9* (46), 25827−25851.
(67) Biermann, O.; Hädicke, E.; Koltzenburg, S.; Müller-Plathe, F. Hydrophilicity and Lipophilicity of Cellulose Crystal Surfaces. *Angew. Chem., Int. Ed.* **2001**, *40* (20), 3822−3825.
(68) Yamane, C.; Aoyagi, T.; Ago, M.; Sato, K.; Okajima, K.; Takahashi, T. Two Different Surface Properties of Regenerated Cellulose due to Structural Anisotropy. *Polym. J.* **2006**, *38* (8), 819−826.
(69) Song, M.; Jiang, J.; Zhu, J.; Zheng, Y.; Yu, Z.; Ren, X.; Jiang, F. Lightweight, strong, and form-stable cellulose nanofibrils phase change aerogel with high latent heat. *Carbohydr. Polym.* **2021**, *272*, 118460.
(70) Arditty, S.; Whitby, C. P.; Binks, B. P.; Schmitt, V.; Leal-Calderon, F. Some general features of limited coalescence in solid-stabilized emulsions. *Eur. Phys. J. E* **2003**, *11* (3), 273−281.
(71) Li, W.; Pham, H. H.; Nie, Z.; MacDonald, B.; Güenther, A.; Kumacheva, E. Multi-Step Microfluidic Polymerization Reactions Conducted in Droplets: The Internal Trigger Approach. *J. Am. Chem. Soc.* **2008**, *130* (30), 9935−9941.
(72) Jiménez Saelices, C.; Capron, I. Design of Pickering Micro- and Nanoemulsions Based on the Structural Characteristics of Nanocelluloses. *Biomacromolecules* **2018**, *19* (2), 460−469.
(73) Cervin, N. T.; Aulin, C.; Larsson, P. T.; Wågberg, L. Ultra porous nanocellulose aerogels as separation medium for mixtures of oil/water liquids. *Cellulose* **2012**, *19* (2), 401−410.
(74) Buchtová, N.; Budtova, T. Cellulose aero-cryo- and xerogels: towards understanding of morphology control. *Cellulose* **2016**, *23* (4), 2585−2595.
(75) Kalashnikova, I.; Bizot, H.; Bertoncini, P.; Cathala, B.; Capron, I. Cellulosic nanorods of various aspect ratios for oil in water Pickering emulsions. *Soft Matter* **2013**, *9* (3), 952−959.

https://doi.org/10.1021/acsomega.3c03871
ACS Omega 2023, 8, 36856−36867

(76) Sing, K. S. W. Reporting physisorption data for gas/solid systems with special reference to the determination of surface area and porosity (Recommendations 1984). *Pure Appl. Chem.* **1985**, *57* (4), 603−619.
(77) Sehaqui, H.; Zhou, Q.; Berglund, L. A. High-porosity aerogels of high specific surface area prepared from nanofibrillated cellulose (NFC). *Compos. Sci. Technol.* **2011**, *71* (13), 1593−1599.
(78) Thommes, M.; Kaneko, K.; Neimark, A. V.; Olivier, J. P.; Rodriguez-Reinoso, F.; Rouquerol, J.; Sing, K. S. W. Physisorption of gases, with special reference to the evaluation of surface area and pore size distribution (IUPAC Technical Report). *Pure Appl. Chem.* **2015**, *87* (9−10), 1051−1069.
(79) Jiang, F.; Hsieh, Y.-L. Assembling and Redispersibility of Rice Straw Nanocellulose: Effect of tert-Butanol. *ACS Appl. Mater. Interfaces* **2014**, *6* (22), 20075−20084.
(80) Mulyadi, A.; Zhang, Z.; Deng, Y. Fluorine-Free Oil Absorbents Made from Cellulose Nanofibril Aerogels. *ACS Appl. Mater. Interfaces* **2016**, *8* (4), 2732−2740.

https://doi.org/10.1021/acsomega.3c03871
ACS Omega 2023, 8, 36856−36867